Mineral. Deposita 28, 291–302 (1993)

Mineralium Deposita

Correlation between chromite composition and PGE mineralization in the Critical Zone of the western Bushveld Complex*

B. Teigler and H.V. Eales**

Department of Geology, Rhodes University, Grahamstown 6140, South Africa

Received: December 18, 1991 / Accepted: June 22, 1993

Abstract. Detailed mineralogical investigations of chromite in the Lower and Critical Zones in the northwestern sector of the Bushveld Complex have revealed significant compositional variations with regard to modal proportions, host-rock lithology, and stratigraphic height. Superimposed on these variations are long-range systematic trends in the composition of chromite in the massive layers. These long-range trends are closely linked with the evolution of the silicate cumulates. The massive chromitite layers are divided into two types. Type 1 comprises the chromitites hosted entirely within ultramafic cumulates, while Type 2 chromitites are within cyclic units in which plagioclase cumulates occur. The types are also distinguishable by their respective contents of platinum-group elements (PGEs) and distribution patterns thereof, viz. the ratios between Ru + Os + Ir and Pt + Pd + Rh, or relative element proportions, both of which display a systematic change with height in accordance with chromite composition. The relation between silicate geochemistry, chromite composition, and PGE tenor, leads to the development of a model explaining the formation of PGE-mineralized, sulphide-poor chromitite layers in the Critical Zone of the Bushveld Complex.

South Africa is a major supplier of chromium ore, which is hosted within the Bushveld Complex (BC) holding ca. 75% of the world's known chromite reserves (Griffith 1989). The BC is one of the largest mafic intrusions on Earth and is subdivided into several compartments (Fig. 1): (a) the far-western lobe, (b) the western lobe, (c) the eastern lobe, (d) the northern lobe, and (e) the Bethal lobe. The cumulate succession is broadly subdivided into the Lower, Critical, Main and Upper Zones on a basis of lithology. The chromium ore is concentrated in numerous layers formed mainly of chromite. These layers vary in thickness, but some are consistent along strike for some 200 km.

The majority of the chromitite layers occur in the Critical Zone of the layered succession and are hosted by both ultramafic and mafic cumulates. Throughout the silicate cumulate pile, chromite is also present as an accessory phase. In recent years, one of the layers (UG2 chromitite) has been exploited for its content of PGEs. However, all the chromitite layers in the sequence studied show an enrichment in PGEs relative to the silicate rocks, although most remain uneconomic under present conditions.

Previous work

In 1865, Mauch noted the occurrence of chromite in South Africa (Silk 1988). Early investigations of the mineralogy of chromite were based on whole-rock samples and wet-chemistry techniques (*inter alia* van der Walt 1941). Van der Walt (1941) analysed chromite from the western BC and described for the first time compositional variations with height. Cousins and Feringa (1964) reviewed earlier work, and in conjunction with their own data, introduced the present well-established stratigraphic grouping of the chromitite layers in the western BC. In the eastern part of the complex, Cameron and coworkers (*inter alia* 1959, 1964, 1974, 1977) studied the chromitite deposits in detail.

The development of techniques of microprobe analysis allowed the composition of chromite to be studied in greater detail without the disturbing influences of gangue, inclusions, or alteration, to which whole-rock analysis is subject. In the western part of the complex Eales and Reynolds (1986) focused on the Upper Group (UG) of chromitite layers, while von Gruenewaldt and Worst (1986) worked on some of the Lower Group (LG) of chromitite layers. The currently accepted model for the formation of chromitite layers may be summarized as a magma-mixing model, where the bulk composition of the resulting hybrid is shifted into the chromite stability

* Presented at the International Conference for Applied Mineralogy, Pretoria, September 1991

** *Present address*: Rio Tinto Namibia (Pty) Ltd., P.O. Box 1079, Windhoek, Namibia

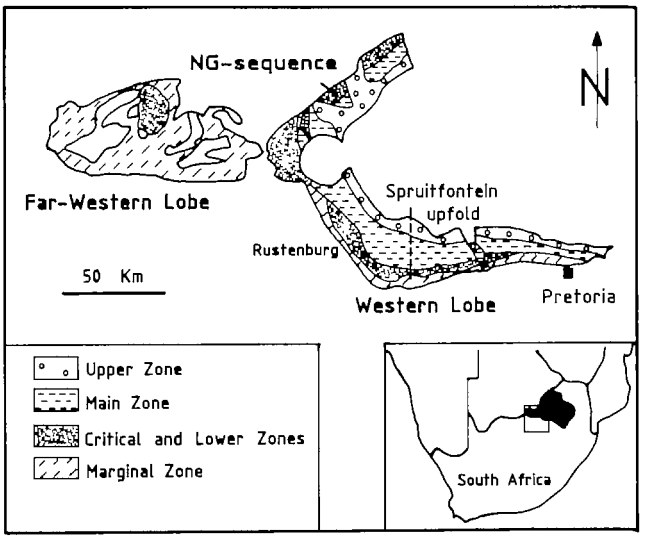

Fig. 1. The western Bushveld Complex and the location of the study sequence

field (Irvine 1975, 1977; Irvine et al. 1983). The reader is referred to Hatton and von Gruenewaldt (1987) for a comprehensive review on the geological setting and petrogenesis of the Bushveld chromitite layers.

The importance of chromite as a petrogenetic indicator was indicated by Irvine (1965, 1967), who concluded that chromite has generally formed simultaneously with olivine and that the crystallization of chromite has been determined in many occurrences by a reaction-forming pyroxene. Eales et al. (1980) described the evolution of spinel in Karoo dolerites and gabbros in terms of four stages: (a) an early stage in which Cr-rich spinel trends towards more Al-rich compositions because of the coprecipitation of olivine; (b) a middle stage, characterized by the onset of the crystallization of plagioclase, thus depleting the liquid in Al_2O_3; (c) a late stage marked by a sharp decrease in Cr in the liquid by virtue of nucleation of clinopyroxene, which is an effective scavenger of Cr; and (d) a final stage characterized by the crystallization of Ti-magnetite. Between stages (c) and (d), a hiatus in the crystallization of spinel might occur, the so-called 'spinel-gap'. The primary composition of the crystallizing spinel is thus dependent on (a) the composition of the liquid, (b) coprecipitating phases, (c) the temperature and pressure (*inter alia* Hill and Roeder 1974), and (d) the oxygen fugacity (Ulmer 1969). A significant complication arises from the modification of primary cumulus compositions, by processes of postcumulus re-equilibration, described *inter alia* in Bushveld deposits by McDonald (1967), Cameron (1975), and Eales and Reynolds (1986). Roeder and Campbell (1985) found that chromite compositions can be related to the purity of the cumulates and to the nature of the surrounding silicate mineral. Their data suggested that in ad- and mesocumulates, chromite displays a restricted compositional range (high in Mg, Al and Cr). In orthocumulates chromite shows enrichment in Fe and Ti. Roeder and Campbell also described the ability of chromite to equilibrate with the interstitial liquid if the grains were enclosed in olivine. No obvious correlation between grain size and composition was found by them for grains within a particular silicate phase. Botha (1987) reported a similar TiO_2 enrichment in grains interstitial to orthopyroxene or included in postcumulus plagioclase, but established a link between the grain size and Ti content.

In recent years, much work has focused on PGEs and their distribution in chromite-rich rocks. Scoates et al. (1988) divided the PGEs into two groups. The Ru group (Ru, Os and Ir; hereafter Σ Ru) is, according to these authors, associated with chromite, and the most likely platinum-group mineral (PGM) is laurite. The Pt group (Pt, Pd and Rh; hereafter Σ Pt) is associated mainly with interstitial base metal sulphides (BMS) and only in a minor degree with chromite. The close spatial PGE-chromitite relation was described by von Gruenewaldt et al. (1986), Naldrett and von Gruenewaldt (1988), and Lee and Parry (1988). Teigler (1990a, 1990b) recorded a geochemical relationship between the mineralogy of chromite and relative proportions of PGE in a section through the western BC.

Analytical techniques

All mineral analyses were performed on an automated JEOL CXA-733 electron-probe microanalyser using a variety of international standards as well as pure synthetic crystals for calibration. Most of the work on chromite was done with a focused 1 μm beam, an operating voltage of 15 kV, and a beam current of 25 nA. The counting times were set at 30 s for the peak position and 10 s for the background position. Long-term machine drift was monitored by the use of a secondary standard. The analytical precision was tested by ten closely spaced analyses in the core domain of an unzoned grain of chromite. Coefficients of variation (calculated as 100 × standard deviation/mean concentration) are in the region of 0.31% for major components, but increase as the absolute levels decline. Accordingly, the coefficients are 0.5 – 1.0% for concentrations within the range of 5 – 20 wt% and rise above 1% as the absolute levels approach the level of 1 wt%. The analyses for PGEs and Au were done by Sheen Analytical Services Ltd, Australia, using ICP-mass spectrometry after a Ni-sulphide collection technique. Duplicate analyses yielded acceptable analytical precision.

Location and lithostratigraphy of the sequence under review

The study sequence (hereafter NG-sequence, after the farm Nooitgedacht, on which the drilling was executed) is situated in the northwestern sector of the complex (Union Section, RPM; Fig. 1). The NG-sequence intersected (Fig. 2) is ca. 1800 m thick and comprises mainly orthopyroxenites (hereafter pyroxenites) and olivine-rich cumulates (dunites and harzburgites), with minor norites and anorthosites in an interval (ca. 60 m thick) below the uppermost chromitite layer intersected (Middle Group (MG) 4 chromitite). A noritic layer, ca. 2 m thick, occurs also at a depth of ca. 1340 m. The sequence is subdivided

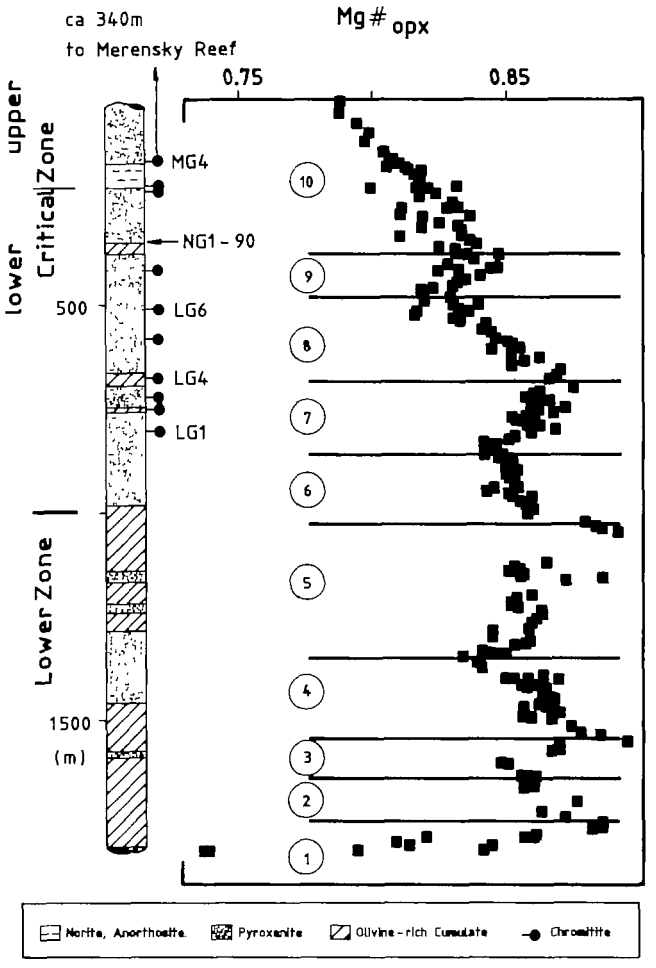

Fig. 2. The variation of $Mg\#_{opx}$ through the NG-sequence. *Numbers in circles* identify segments (for further details see Teigler, 1990b, and Eales et al. 1990b)

according to the informal zonal subdivision (SACS 1980) into the Marginal Zone, (lowermost 30 m), the Lower Zone (LZ, the lower half of the NG-sequence, see Fig. 2), and part of the Critical Zone (CZ). The appearance of cumulus plagioclase in the CZ defines the boundary between the lower (lCZ) and the upper Critical Zone (uCZ), while the boundary between CZ and LZ was redefined by Eales et al. (1990b) as the top of the uppermost thick olivine-rich package below the thick pyroxenitic unit hosting the LG1 chromitite. In the CZ of the NG-sequence, ten prominent chromitite layers are present, which are readily correlatable with the LG1 to MG4 chromitite succession of Cousins and Feringa (1964), although no thick MG1 chromitite appears to be developed in the northwestern sector of the western BC (see also Hatton and von Gruenewaldt 1987).

In Fig. 2, the variations in Mg # (Mg/(Mg + Fe)) of orthopyroxene through the NG-sequence are displayed to illustrate the overall evolution of the silicate cumulates. The range of $Mg\#_{opx}$ is between 0.737 and 0.894. By means of this ratio, the cumulate pile can be subdivided into ten segments, depending on whether Mg # increases or decreases with height. The lower portion (segments 1–5), with an overall increase of Mg #, can be equated with the Marginal and Lower Zones, while the upper portion (segments 6–10), characterized by a general decrease, is part of the CZ. Further details of this variation through the succession are given in Eales et al. (1990b).

Mineralogy of chromite

Chromite is the most common accessory cumulus phase throughout the entire sequence. Chromite-free lithologies are, in fact, very rare and are limited to intervals in the uCZ (above the MG4 chromitite) and the LZ (in the vicinity of the leuconorite at a depth of ca. 1340 m).

A detailed study of crystal zonation was not attempted, but sporadic core-rim pair analyses were made to detect geochemical gradients. The majority of grains do not show significant or systematic zonal structure (Table 1). Intra-sample variations are more significant, when chromite grains included in orthopyroxene are compared with interstitial grains (Table 1). The latter are generally enriched in Ti and Fe, but depleted in Al and Cr; other major elements are in unchanged concentrations. These findings are in agreement with the results of Botha (1987) and Roeder and Campbell (1985). However, not all the grains analysed follow such general trends, and the influence of coprecipitating phases like Ti-rich mica might shift chromite compositions in the interstices to very low Ti values. In summary, each analysis of chromite may represent partial or complete subsolidus equilibration, and it is a function of the composition of the magma, temperature, pressure, oxygen fugacity, reaction with residual liquid, and element partitioning between phases. It is obvious that, in re-equilibration, the ratio of phase: liquid is of major importance, i.e. the modal proportions of the coexisting phases have to be considered. Because of this complexity, it is difficult to assess the composition of chromite that represents the least-modified, near-liquidus composition, and so all the chromite analyses of each sample were averaged to give a composition 'representative' of each sample. A total of 213 samples (1142 analyses) were used to compile the diagrams and tables presented. The Fe_2O_3 concentrations were calculated on the assumption of stoichiometric distribution of the cations.

In the conventional triangular diagrams (Fig. 3) depicting the trivalent cations, the compositional variations of chromite in the NG-sequence are illustrated. The following general observations emerge: (a) chromite in massive layers is poorer in Fe^{3+} than chromite modally present in accessory or major proportions (Fig. 3A) – Cameron (1977) reported a similar depletion in chromite from chromitites in the Eastern BC; (b) chromites of massive layers hosted within the uCZ (Fig. 3A) have distinctly higher concentrations of Al than chromites of massive layers in the ICZ (Fig. 3B), despite the juxtaposition with plagioclase cumulates; (c) chromite hosted by olivine-rich rocks shows elevated concentrations of Al (Fig. 3C and Fig. 4), as predicted by Eales et al. (1980) and described in the Western BC by Botha (1987) and in the Great Dyke of Zimbabwe by Wilson (1982); and (d) accessory chromite hosted by norites and anorthosites in the uCZ is conspicuously depleted in Al, indicating the influence of crystallization of plagioclase (Fig. 3B). This

Table 1. Selected microprobe analyses of chromite (core and rim domains)

Sample	NG1-569.20				NG1-197.50				NG1-327.45				NG1-29.80		NG1-55.40		NG2-773 90	
Habit	Int		Incl		Int		Incl		Incl		Int		Incl	Int	Incl	Int	Int	Incl
Size (in μm)	50		10		290		90		130		150		50	200	60	200	110	80
Domain	Core	Rim	Core	Rim	Core	Rim	Core	Rim	Core	Rim	Core	Rim	Core	Core	Core	Core	Core	Rim
wt.Z																		
TiO_2	0.71	0.41	0.13	0.14	0.69	0.68	0 23	0.21	0.65	0.53	0.73	0.70	0.48	0.91	0.58	1.17	0.90	0.59
Al_2O_3	7.75	7.71	7.69	7.60	9.34	9.42	12.80	12.24	10.25	10.31	8.88	8.40	11.49	8 32	10.59	9.17	7.24	9.85
Cr_2O_3	50.79	49.51	51.14	49.23	46.96	47.08	45.71	47.34	47.50	48 16	48 98	50.04	45.23	46.00	43.53	42.20	44.39	48.72
FeO	25.50	25.06	25.62	25.02	25.19	25.13	26.01	26.17	25.23	25.32	25.38	25.55	25 60	26.27	26.03	26.17	30.82	29.02
Fe_2O_3	8.45	9.06	9.38	10 16	11.14	10.82	9.31	8 72	10.17	9.94	8.92	8.65	10.97	13.30	13.88	16.42	12.45	7.40
MnO	0.43	0 35	0.38	0.36	0.29	0.31	0.26	0.30	0.38	0.36	0.37	0.39	0.38	0.33	0 42	0 35	0 36	0.32
NiO	0 17	0 06	0.09	0.08	0 15	0.12	0 10	0.10	0.12	0.14	0.17	0.16	0 10	0.13	0.18	0.26	0.08	0.09
MgO	4.75	4.59	4.46	4 49	5 27	5 28	4.97	4.90	5 44	5.41	4.95	4.84	5 16	4.77	4.89	5.12	1.14	2.76
Total	98.55	96.74	98.90	97.08	99.05	98.85	99.40	99 99	99.75	100 16	98.38	98.73	99.40	100.03	100 10	100.87	97.37	98.74
Cations (based on 32 oxygens)																		
Ti	0.152	0.088	0.028	0.030	0.144	0.141	0.048	0.043	0.135	0.110	0.154	0.148	0.098	0 190	0.121	0.242	0.198	0.125
Al	2.576	2.613	2 556	2.571	3.060	3.091	4.121	3 930	3 317	3.323	2.938	2 777	3.719	2.726	3.430	2.966	2.512	3.283
Cr	11.327	11.251	11.399	11.173	10.321	10.360	9 870	10.196	10 311	10.414	10.869	11.101	9.819	10.111	9.459	9.159	10.334	10.893
Fe^{2+}	6 016	6.023	6.041	6.005	5.856	5 849	5.941	5.963	5.703	5 790	5.959	5.995	5.878	6.106	5.981	6.008	7.589	6.864
Fe^{3+}	1.794	1 960	1.990	2.196	2.331	2.267	1.913	1.788	2.102	2.045	1.884	1.826	2.266	2 783	2.870	3.392	2.758	1.575
Mn	0.102	0.084	0.090	0.087	0 069	0.074	0.061	0.070	0.088	0 084	0 087	0.093	0.087	0.078	0.097	0.081	0.091	0.077
Ni	0.038	0.014	0.021	0.019	0 034	0.027	0.022	0.023	0.027	0 030	0 038	0.035	0.022	0.029	0.041	0.058	0.020	0.200
Mg	1 996	1 968	1.876	1.920	2.185	2.191	2 025	1 988	2.227	2.206	2.071	2.025	2 111	1.977	2.002	2.095	0.499	1.164
Cationic ratios																		
Cr/Al	4 397	4.306	4 460	4.346	3 372	3.352	2.395	2.595	3.109	3.134	3.700	3.997	2.640	3.710	2.758	3.088	4.114	3.318
Mg #	0.249	0.246	0.237	0.242	0.272	0.273	0.254	0.250	0.278	0 276	0.258	0.253	0.264	0.245	0.251	0.259	0.062	0.145
FFE	0.230	0 246	0.248	0.268	0.285	0.279	0 244	0.231	0.266	0.261	0.240	0.233	0.278	0.313	0 324	0.361	0.267	0.187
Cr/Cr + Al	0.815	0.812	0.817	0.813	0.771	0.770	0 706	0.722	0.657	0.758	0.787	0 800	0.725	0.788	0 734	0.755	0.804	0.768
Weight ratio of metals																		
Cr/Fe	1 350	1 312	1.322	1.269	1 174	1.189	1.170	1.225	1.216	1.234	1.290	1.322	1.123	1.060	0.995	0 907	0.930	1 202

Int, Interstitial with plagioclase as adjacent phase; Incl, Inclusion in orthopyroxene, Mg #, Cationic ratio of $Mg/(Mg + Fe^{2+})$; FFE, Cationic ratio of $Fe^{3+}/(Fe^{3+} + Fe^{2+})$; Cr/Fe, Weight ratio of Cr metal to Fe metal

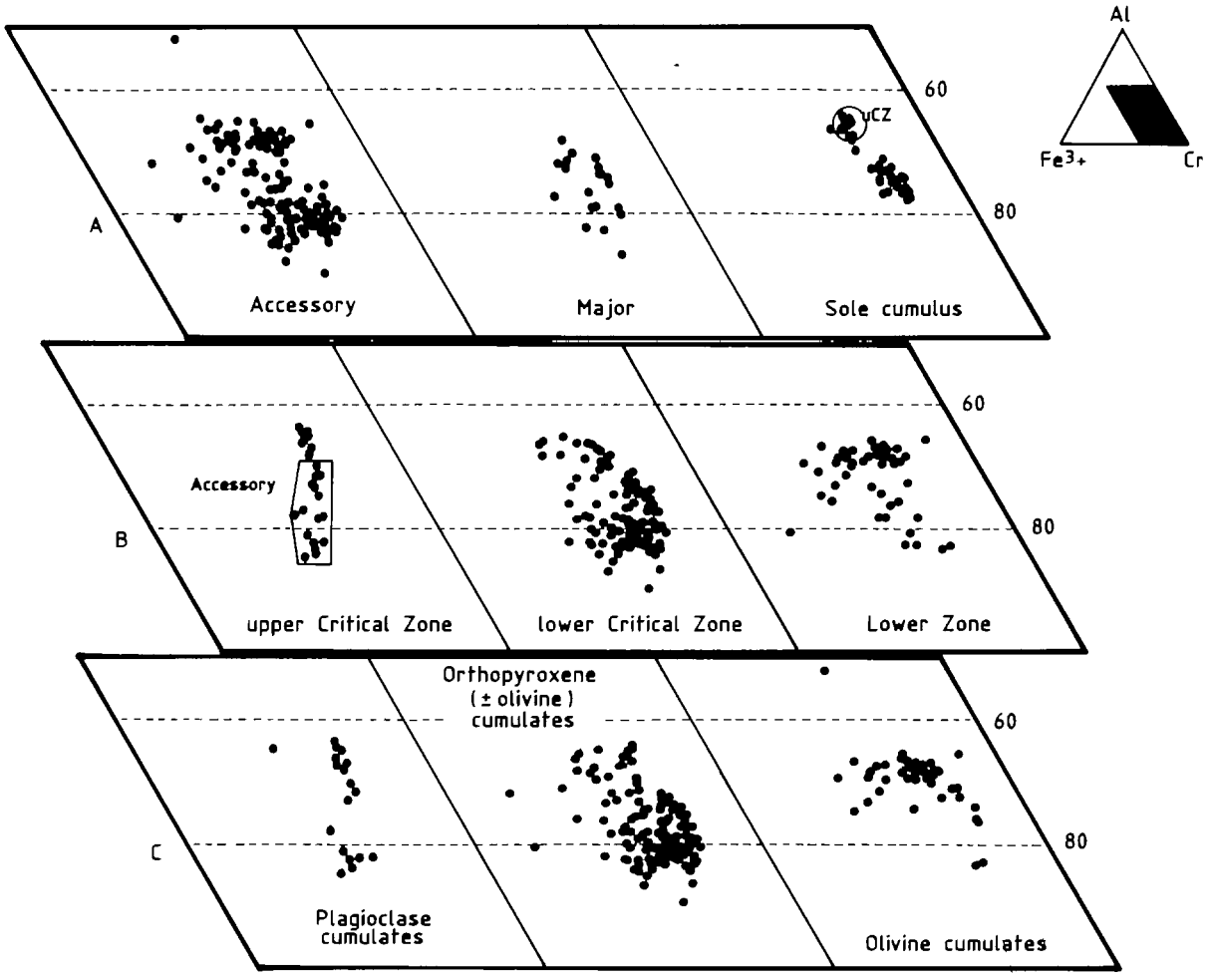

Fig. 3A–C. Conventional triangular diagrams depicting variations in the trivalent cations in chromite in the NG-sequence with: *A* modal proportions, *B* stratigraphic height, and *C* type of host rock

feature is attributed to partitioning between spinel and feldspar.

From Fig. 4, which displays cryptic variations with height, further observations can be drawn: (e) distinctly different chromite compositions are recorded in successive massive layers; (f) the highest values for $Mg\#_{chr}$ (range: 0.40–0.58) are found in chromite from massive layers; (g) chromite in the lCZ is conspicuously enriched in Cr; (h) the FFE ratio ($Fe^{3+}/(Fe^{3+} + Fe^{2+})$) shows wide scatter in the LZ, while, in the CZ, a more limited range is displayed – a general increase with stratigraphic height is initiated above the level of the LG4 chromitite; (i) the Cr/Fe ratio (mass ratio of metals, using total Fe) shows a slight overall increase up to the LG4 chromitite, above which a general decline is apparent; (j) chromite in the massive chromitites of the uCZ appears to contain less Cr than accessory chromite in this zone, while in the lCZ this relationship seems to be reversed.

In the NG-sequence, all LG and MG chromitites (as well as numerous minor chromitites or chromite-rich layers) were intersected. Sample NG1-90 at a depth of 340.33 m (see Fig. 2) is interpreted as the poorly developed MG1 chromitite. In Fig. 5, the average chromite compositions (microprobe data) in each chromitite layer are summarized, together with data for the Merensky Reef chromitite stringers, and the UG2 and UG1 chromitites, from Eales and Reynolds (1986).

The level of Ti (an indicator element for fractionation) increases upwards. This enrichment trend begins above the LG4 chromitite; Fe^{3+} follows a similar distribution pattern. There is no significant variation in the Mn values or the FFE ratio, which implies that the ratio of ferric to ferrous iron remains more or less steady. The most common cations, Cr and Al, display an antipathetic relationship in support of the described cation exchange. At the level of the sample NG1-90 at a depth of ca. 340 m the Al_2O_3 attains levels above 17% by mass (> 5.0 cations) and such high levels of Al are maintained throughout the succeeding chromitites. At the same level, the Cr cations drop below nine and, despite a slight increase towards the UG2 chromitite, this value is not reached again. The Cr levels are highest within the layers associated with or between the olivine-rich intervals. The ratios Cr/Fe and Cr/Al duplicate the trend set by Cr.

In summary, the following conclusions can be drawn: (a) the variations displayed by the massive chromitite layers appear to reflect the chemical evolution of the silicate cumulates by which they are hosted; (b) no consistently uniform, general trend is evident; (c) the appearance of abundant cumulus plagioclase within the sequence

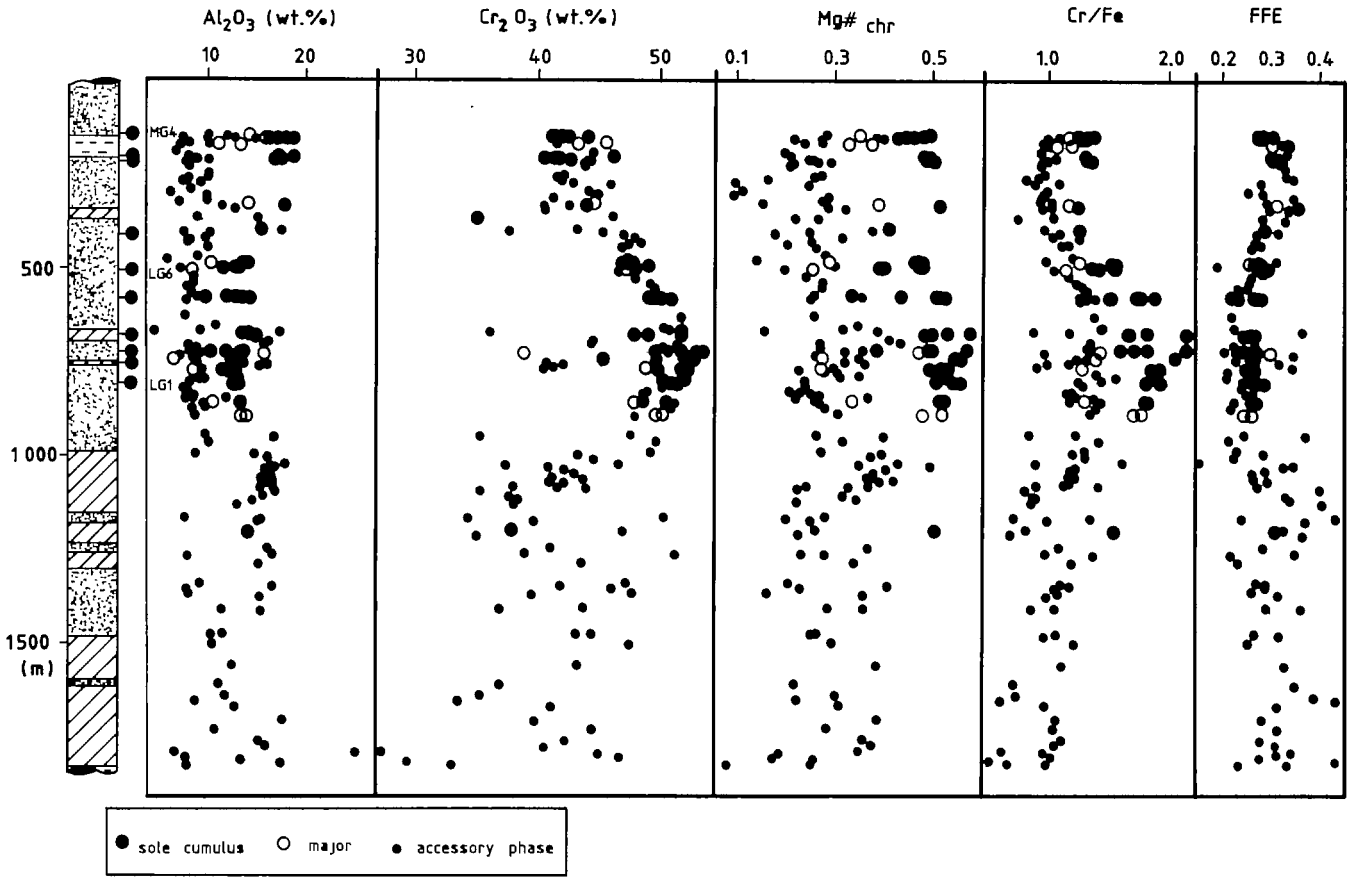

Fig. 4. Cryptic variations of chromite through the NG-sequence (see text for explanations of ratios $Mg\#_{chr}$, Cr/Fe and FFE). Ornamentation for rock types as in Fig. 2

cannot be fixed by the mineralogy in massive layers; a shift to significantly higher values of Al occurs at a stratigraphic level ca. 125 m below the actual boundary between lower and upper CZ. However, relicts of cumulus plagioclase occurring as rounded and resorbed inclusions in orthopyroxene below this boundary point to the possibility of cumulus plagioclase having been present in the liquid at much lower levels (Eales et al. 1990a, 1990b, and 1991); (d) the massive chromitite layers of the NG-sequence can be assigned geochemically to three types (Teigler 1990a, 1990b) which do not correspond with the conventional stratigraphic subdivision into Lower, Middle and Upper groups:

Type 1a: LG1 to LG4 chromitites: Cr/Fe > 1.75; $Fe^{3+} < 1.45$; $Ti < 0.1$
Type 1b: LG5 to MG1 chromitites: Cr/Fe < 1.72; $Fe^{3+} > 1.48$; $Ti > 0.1$
Type 2: MG2 to UG2 chromitites: Cr/Al < 1.73; $Ti > 0.128$.

Whereas Type 1 is hosted entirely by ultramafic cumulates, Type 2 chromitites occur in cyclic units in which plagioclase cumulates are abundant.

Cryptic variations of chromite through individual layers of chromitite appear to be limited. Two layers, the LG6 and MG4 chromitites, were investigated in more detail. Although eight samples through the LG6 chromitite establish an overall increase of the Cr/Fe ratio with height, scrutiny shows a deflection to higher values in the central portion of the layer. No systematic pattern can be seen in other parameters. The variations are, in any case, limited, and for the Cr/Fe ratio a standard deviation of $\pm$ 0.06 of the mean value of 1.55 was calculated. Through the MG4 chromitite (eight samples), interpretation is hampered by a pyroxenitic parting (ca. 2.2 m thick) splitting the layer into the MG4A and MG4B chromitites. Again, a general increase in the Cr/Fe ratio and Ti with height might be present, but no trend in the Cr/Al ratio is evident.

The relationship between chromite composition and PGE contents

For the sequence studied, no microprobe or mineragraphic study of the platiniferous phases was done, but earlier work by Teigler (1990a) supports the grouping of the PGEs, as proposed by Scoates et al. (1988), in the

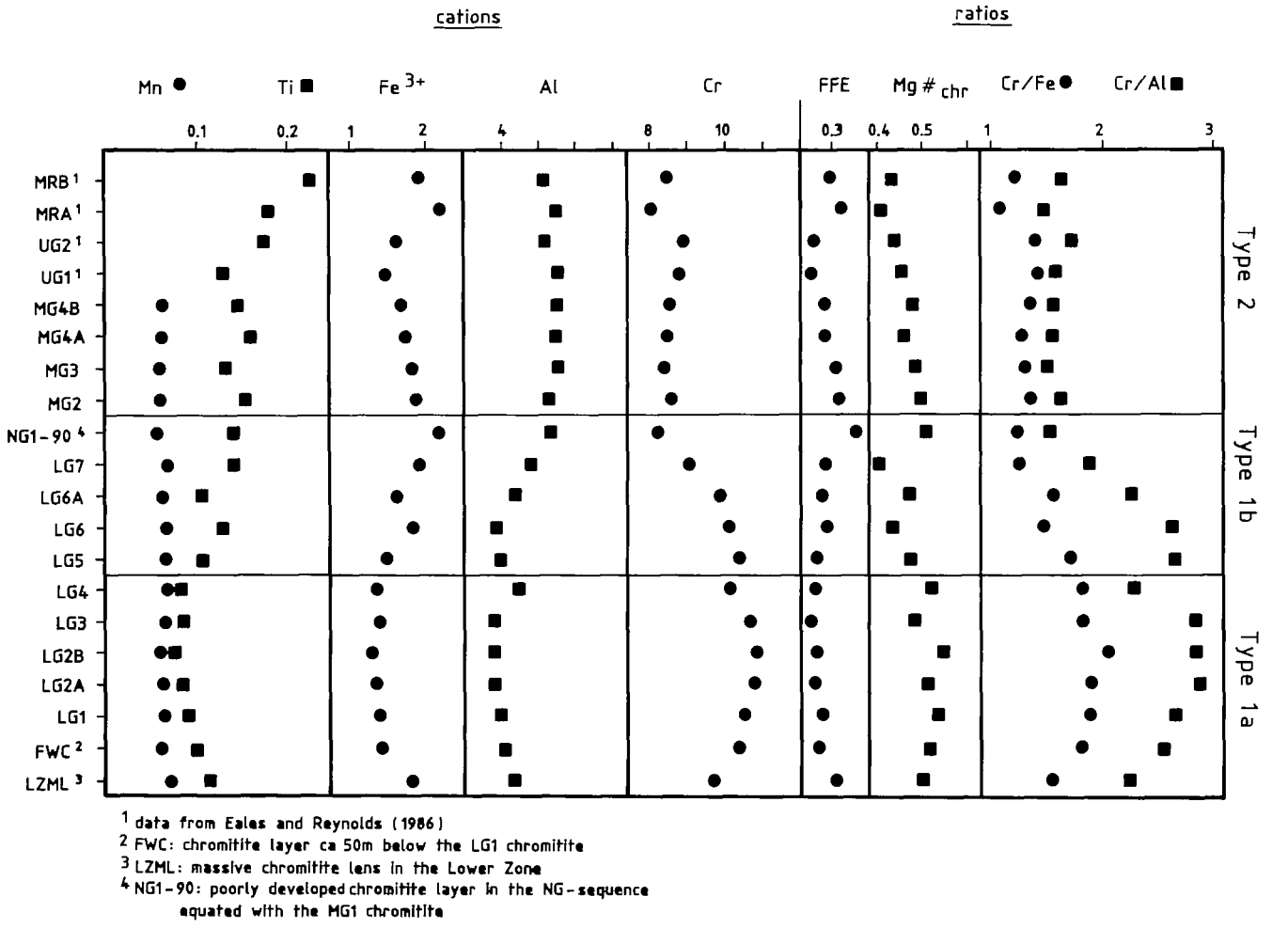

Fig. 5. Average compositions of chromite from chromitite layers at Union Section (*solid lines* depict type boundaries). Ratios are explained in the text

chromitites of the BC. For the purpose of this paper, and for simplicity, all the figures and tables presented here will therefore depict the distribution of ΣRu and ΣPt and the ratios between them.

The PGE concentrations through the NG-sequence are illustrated in Fig. 6. The background concentration was established by analysis of 18 silicate cumulates. It is evident from the diagram that no significant change in the background levels occurs with height (average total PGEs (ΣPGE) + Au = 75 ppb). In contrast, the average weighted PGE contents of the massive chromitite layers show a profound if irregular increase of ΣPGE with height.

In plots of PGE levels against selected geochemical parameters of chromite (Fig. 7), a three-field distribution is evident, as outlined by Teigler (1990a). Although the distribution patterns lack overall good statistical correlation, the salient features are the following.

1. A negative correlation exists between ΣPt and the ratios Cr/Fe and Cr/Al of chromite, while ΣRu appears to be positively linked.
2. Using Ti (cations) as the abscissa reverses these relationships.
3. The Type 1a chromitite layers with the most primitive traits (i.e. high Cr/Fe and Cr/Al, and low Ti) generally contain the lowest concentrations of PGEs. Here the PGE content comprises 70.6% ΣRu and 29.4% ΣPt with a standard deviation of 10.8% (see Table 2). Within ΣRu, Ru is the most abundant element (77.1% ± 5.7%), and Os and Ir are present at equal levels (10.9% ± 2.2% and 12.0% ± 5.0%, respectively). Surprisingly, Rh is relatively the most abundant species in ΣPt (43.6% ± 3.3%), although the relative abundance of Pt is very similar (38.5% ± 6.4%). The proportion of Pd averages 17.9%.
4. Within samples from the Type 1b chromitites of the intermediate field, ΣPGE may reach up to 1.4 ppm. In this type the ΣRu constitutes 46.2% ± 10.6%, while ΣPt is 53.8% ± 10.6%. The intra-group relative abundances are listed in Table 2. In ΣRu, Ru is the most abundant element, followed by Os and Ir in broadly equal proportions. In ΣPt, Pt is now the most abundant PGE, followed by Rh.
5. The Type 2 chromitite layers with the most evolved characteristics (low Cr/Fe and Cr/Al, and high Ti) display higher PGE contents than those of the Type 1, notably in the UG2 chromitite. The ratio ΣPt:ΣRu is now approximately 80:20 (see Table 2). In ΣRu, Ru is still present in highest proportion, but lower in absolute levels than in Type 1. The levels of Ir are significantly high in some samples of the MG chromitites. In ΣPt, Pt displays the

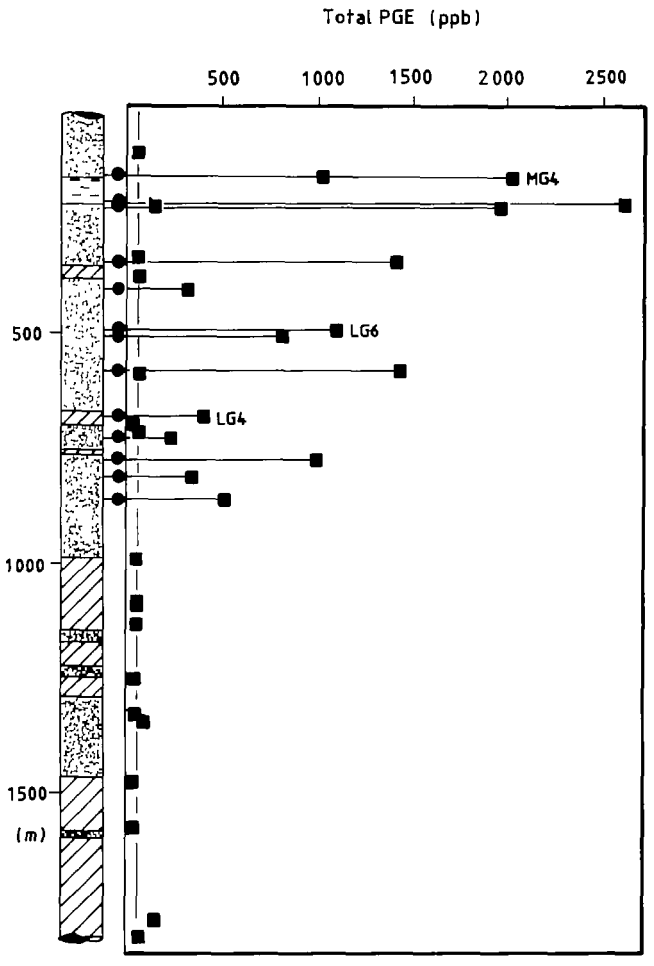

Fig. 6. The total PGE distribution (*squares*) through the NG-sequence. The *dashed line* denotes the average PGE content of the silicate samples, and the *filled circles* the positions of chromitite layers

highest relative concentrations. From Table 2 it is not clear if Rh or Pd is the more abundant. It appears that, in samples from the MG chromitites, Rh is present in higher proportions than Pd, while, in the UG2 chromitite, this relationship is reversed. From the relatively higher proportions of Rh and Ir in some samples of the MG chromitites, it might be concluded that an Ir-Rh phase is present here. Von Gruenewaldt et al. (1986) reported the occurrence of one of such possible phase (irarsite, an Ir-Rh-As-S mineral) in the MG2 chromitite in the southern sector of the western BC.

From Table 2, it is evident that the relative abundance of Ru, Ir, Rh, Pd and Pt varies in accordance with the composition of chromite, whereas the proportion of Os does not change significantly. This pattern, as well as the grouping, is also readily recognizable in Table 3, which shows the average weighted proportions of PGEs in the successive chromitite layers. However, the PGE tenor in two chromitite layers (sample NG1-90 and the LG7 chromitite) produces some overlap between Type 1b and Type 2 chromitites. Here, the ratio $\Sigma Pt:\Sigma Ru$ is very similar to that from chromitites higher up in the sequence, but the proportion of Ru shows more resemblance to Type 1b chromitites. The latter feature, the chromite composition and stratigraphic position justify their assignment to Type 1. These two layers are also abnormal by virtue of their juxtaposition to olivine-rich cumulates, a somewhat unusual rock type at these stratigraphic levels.

Because of the limited variations of the composition of chromite within chromitite layers, no correlation between mineralogy of chromite and the distribution of PGEs might have been anticipated. However, from Table 4, it is evident that many correlation coefficients are better than 0.5, and, for the LG6 chromitite, better than 0.65. This points strongly to a correlation between the distribution of PGEs and the composition of chromite.

Discussion and conclusions

Compositional differences are greater between accessory chromite and chromite present in rock-forming proportions than between chromite present in major proportions, and as the sole cumulus phase (i.e. in the massive chromitites). Accessory chromite displays a strong compositional dependence upon the host rock. In association with plagioclase cumulates it is depleted in Al, but in olivine-rich lithologies it shows elevated levels of Al. Most of the chromite in pyroxenites covers an intermediate field, a feature that is probably related to the greater compatibility of Al in the orthopyroxene lattice when compared with olivine, but which in turn is low when compared with plagioclase. This systematic pattern cannot be explained by subsolidus equilibration, and is interpreted in terms of coprecipitation of chromite and the respective silicate phases. In other words, chromite as a late accessory phase competed with the major silicate phases for Al, and its levels of Al are therefore greatly dependent on the partition coefficient of Al in the contemporary silicate phases. In contrast, chromite from massive layers does not show a decrease in Al in the uCZ dominated by plagioclase cumulates, but does show steady levels after an initial increase some 125 m below the first appearance of cumulus plagioclase. This pattern we attribute to the early precipitation of chromite alone, which eventually led to the formation of massive layers upon deposition.

The long-range trends in the composition of chromite in successive chromitite layers reflect the evolution of the cumulate succession. Chromitites with the most primitive chromite compositions (Type 1a) are found within segment 7 of Fig. 2, which comprises olivine-rich cumulates and pyroxenites with the highest $Mg\#_{opx}$ in the lCZ, while the most evolved chromitite layers (Type 2) are found within segment 10 and above, in which $MG\#_{opx}$ decreases steadily to values below 0.8. This long-range gradation in both the composition of silicate cumulates and the mineralogy of chromite clearly casts doubt on any models involving long-range gravitational settling, or sporadic chromite-laden density currents. Eales and Reynolds (1986) came to similar conclusions in their study of the chromitites in the uCZ of the western BC. The mixing of liquids near the crystalline floor of the chamber, as was suggested by Irvine (1977), appears to be the most likely process to trigger copious precipitation of chromite.

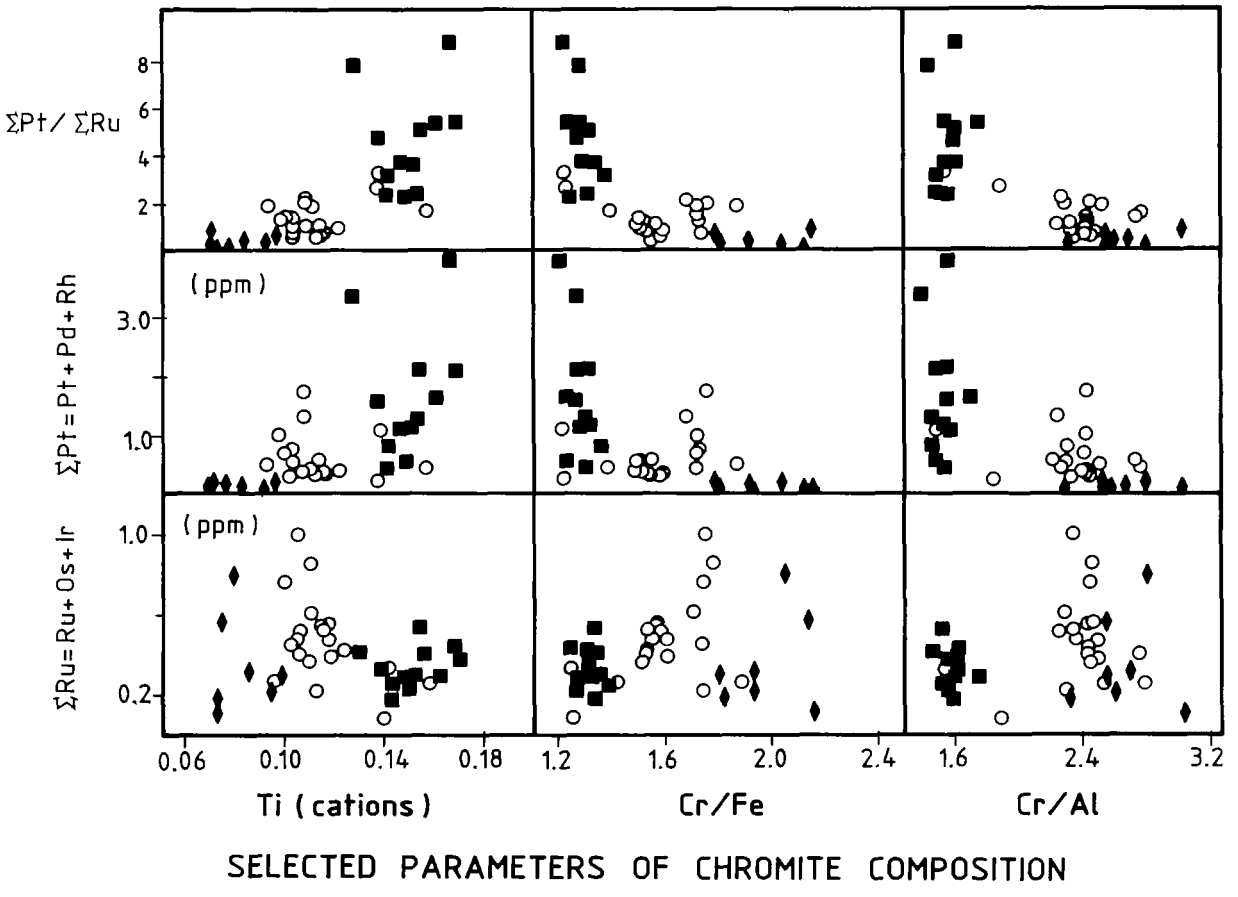

Fig. 7. Correlation between chromite composition and PGE distribution in the chromitite layers (*diamonds*: Type 1a chromitites, *circles*: Type 1b chromitites, and *squares*: Type 2 chromitites)

Table 2. The distribution of ΣRu and ΣPt and their intra-group proportions (all in %) in the different types of chromitite layers. For this tabulation, all the chromitite samples were used

	Type 1a	Type 1b	Type 2[a]	UG2 chromitite Union[b]	Western Plats[c]
ΣRu	70.6 ± 10.8	46.2 ± 10.6	20.5 ± 6.7	16.1	22.1 ± 7.8
ΣPt	29.4	53.8	79.5	83.9	77.9
Os	10.9 ± 2.2	13.3 ± 2.9	16.5 ± 2.2	7.5	
Ir	12.0 ± 5.0	14.6 ± 2.3	36.7 ± 8.6	26.9	
Ru	77.1 ± 5.7	72.0 ± 3.6	46.8 ± 10.2	65.6	
Rh	43.6 ± 3.3	26.2 ± 5.3	20.2 ± 6.4	10.7	8.8 ± 15.5
Pt	38.5 ± 6.4	60.4 ± 8.7	62.9 ± 11.5	64.5	63.5 ± 14.4
Pd	17.9 ± 7.1	13.3 ± 6.5	16.9 ± 7.7	24.8	27.7 ± 14.1

[a] UG chromitites excluded; [b] Data from von Gruenewaldt et al. (1986); [c] Data from Hiemstra (1986)

In the NG-sequence all the massive chromitite layers are enriched in PGEs regardless of their stratigraphic positions. This is in agreement with the data of Lee and Parry (1988) and von Gruenewaldt et al. (1986), who found that the chromitites in their respective study areas are enriched in PGEs relative to associated silicate rocks. This enrichment indicates that the process of entrapment of PGEs operated in each of the chromitite-forming events. Current models for the formation of stratiform deposits of PGEs (Campbell and Naldrett 1979, and Campbell et al. 1983) are based mainly on the Merensky reef, in which chromite is concentrated generally in millimetre-thick layers and, hence, is to be regarded as an accessory phase of the entire mineralized 'reef'. Another characteristic feature is the abundance of BMS in the Merensky Reef. This high proportion of BMS is not matched in the chromitites, which are generally sulphur-poor (Hiemstra 1985, and von Gruenewaldt et al. 1986). The enrichment of PGEs in the chromitite layers may thus have occurred without bulk sulphur saturation, in contrast with the Merensky Reef, where bulk sulphur saturation was probably responsible for the crystallization of BMS and the scavenging of associated PGEs. However, different studies of PGM (von Gruenewaldt et al. 1986,

Table 3. The distribution of ΣRu and ΣPt and their intra-group proportions (all in %) in the chromitite layers of the NG-sequence (included are published data for the Merensky Reef, UG2, and UG1 chromitites). For this tabulation, the weighted average contents of PGEs in the chromitites were used. The listing from left to right reflects the stratigraphic order from bottom to top

	Type 1a chromitites		Type 1b chromitites						Type 2 chromitites						Merensky Reef
	FWC[a]	LG1	LG2	LG3	LG4	LG5	LG6	LG6A	LG7	MG1[b]	MG2	MG3	MG4A	MG4B	UG1[c]	UG2[c]	
ΣRu	59.3	66.3	81.6	60.5	80.9	37.8	55.2	47.8	27.5	23.8	18.3	14.5	22.4	25.1	27.7	16.1	9.9
ΣPt	40.7	33.7	18.4	39.5	19.1	62.2	44.8	52.2	72.5	76.2	81.7	85.5	77.6	74.9	72.3	83.9	90.1
Os	11.2	10.2	14.9	9.8	9.2	12.3	15.0	12.6	11.5	12.0	18.3	16.7	18.1	14.8		7.5	11.3
Ir	9.6	10.4	11.8	16.2	8.7	14.0	13.8	15.4	21.8	22.2	40.3	37.5	39.4	27.3		26.9	19.6
Ru	79.2	79.4	73.3	74.0	82.1	73.7	71.2	72.0	66.7	65.8	41.4	45.8	42.1	57.9		65.6	69.1
Rh	44.2	44.8	43.6	38.0	42.8	26.1	26.0	18.2	23.1	14.0	15.0	20.1	21.2	24.9	12.0	10.7	4.7
Pt	48.1	31.5	47.5	40.8	34.6	58.4	65.0	71.4	39.3	64.5	67.2	45.4	67.5	56.2	54.5	64.5	66.5
Pd	7.7	23.7	8.8	21.2	22.6	15.5	9.0	10.4	37.6	21.5	17.8	34.5	11.2	18.8	33.5	24.8	28.8

[a] FWC, First massive chromitite layer, ca 50 m below the LG1 chromitite; [b] MG1, poorly developed chromitite layer at a depth of ca 340 m (sample NG1-90); [c] data from von Gruenewaldt et al. (1986). UG1 chromitite from the eastern part of the BC

and Merkle 1987) reported that, in chromitites, the majority of PGMs are sulphides, although alloys, tellurides, arsenides, etc., also occur. This obvious paradox, namely sulphide crystallization without bulk sulphur saturation, is regarded as the key to the origin of PGE mineralization in the chromitites. It is suggested that copious crystallization of chromite changed the solubility of sulphur in the silicate melt and triggered the precipitation of the sulphides in the immediate vicinity of the crystallizing chromite. A similar mechanism was proposed by Talkington et al. (1983) for the origin of inclusions of PGMs in chromite of the Bird River sill, by Buchanan (1976) for sulphide and oxide assemblages in the BC, and by Page (1971) for the H chromitite in the Stillwater Complex.

The correlation of the composition of chromite with PGE contents, and distribution patterns on a megascale (viz. through the entire succession of chromitite layers), now merits further attention. Despite a probably continuous crystallization of laurite, no depletion of ΣRu can be detected through the chromitite succession (Teigler 1990a), although the relative proportion of the ΣRu decreases with height. The proportion of ΣPt increase with height. This enrichment can be attributed to a process of fractionation of the PGEs, i.e. the enrichment of ΣPt within the supernatant liquid during the earlier stages dominated by the crystallization of laurite, and accumulation within the massive layers. Because of the lack of bulk sulphur saturation in the silicate melt (reflected by the paucity of BMS in the chromitites as well as silicate cumulates deposited beneath the Merensky Unit), sulphur would also be accumulated in the supernatant liquid. This progressive enrichment in both sulphur and ΣPt would then have caused the increasing degree of mineralization with height that characterizes the chromitite layers. Slight changes in the sulphur content of the replenishing primitive liquids cannot be excluded, and the saturation in sulphur at the level of the Merensky Reef could indicate that, with the progressive evolution of the complex, relatively high-sulphur magmas entered the chamber. It must be conceded that continuous melting of a mantle source would also cause changes in the PGE tenor of the putative parental liquids (Naldrett and Barnes 1986), and this could also produce variations in the distribution pattern of the PGEs.

All the findings can be summarized in a model for the genesis of primary PGE mineralization associated with sulphide-poor chromitites (as distinct from the formation of the sulphide-rich but chromite-poor Merensky Reef) and the possibility of a late-stage postcumulus overprint and redistribution of the mineralization. It is suggested that, after major influxes of pristine and sulphur-undersaturated magma into the chamber, mixing with the supernatant liquid may have occurred so as to shift the bulk saturation of the hybrid liquids into the primary field of chromite. Copious nucleation of chromite dramatically changed the solubility of sulphur in the hybrid silicate liquid, and high-temperature PGMs, mainly laurite and alloys, were formed. When the precipitation of chromite ceased, the saturation of sulphur in the silicate liquid ceased, and sulphur and PGEs behaved once more as incompatible elements, leading to their enrichment in the supernatant liquid. During each event leading to the

Table 4. Correlation coefficients yielded by linear regression of selected parameters expressing chromite composition, and PGE distribution through the LG6 and MG4 chromitites

	LG6 chromitite $n = 8$			MG4 chromitite $n = 8$			MG4A chromitite only $n = 5$		
	Cr/Fe	Cr/Al	Ti	Cr/Fe	Cr/Al	Ti	Cr/Fe	Cr/Al	Ti
ΣRu	0.717	0.753	− 0.701	− 0.133	− 0.417	0.490	0.350	− 0.637	0.217
ΣPt	− 0.833	0.654	0.669	− 0.541	0.123	0.803	− 0.455	0.010	0.793
ΣPt/ΣRu	− 0.926	0.905	0.877	− 0.579	0.541	0.811	− 0.568	0.519	0.831

formation of a chromitite layer, this process was repeated. Absolute and relative abundances of the PGEs changed with height in consequence of progressive fractionation of the residual liquid. Despite the simplicity of the proposed model, it accounts for the most significant features of the PGE-chromitite association: (a) the close spatial relation of PGMs, especially laurite, with chromite, (b) the invariably sulphide-poor character of the chromitite layers in the BC, (c) the gradational changes with height in the mineralogy of orthopyroxene and chromite, and (d) the absolute and relative trends of PGE concentrations in the CZ of the BC.

Acknowledgements. The authors would like to thank the FRD for its financial support during this investigation. GENMIN's cooperation in the form of underwriting the costs of the PGE analyses, and permission to publish the data, is gratefully acknowledged. C. Liebenberg is thanked for her help in finishing the figures.

References

Botha, M.J. (1987) Petrology and geochemistry of the lower group chromitites and host rocks on the farm Zandspruit 168 JP, western Bushveld Complex. Unpublished M.Sc. thesis, Rhodes University, South Africa, pp. 216

Buchanan, D.L. (1976) The sulphide and oxide assemblage in the Bushveld Complex rocks of the Bethal area. Trans. Geol. Soc. S. Afr. 39:76–80

Cameron, E.N. (1964) Chromite deposits in the eastern part of the Bushveld Complex. In: Haughton, S.H. (ed) The geology of some ore deposits in Southern Africa, vol. II. Geol. Soc. S. Afr. Johannesburg 131–168

Cameron, E.C. (1975) Postcumulus and subsolidus equilibration of chromite and coexisting silicates in the eastern Bushveld Complex. Geochim. Cosmochim. Acta 39:1021–1033

Cameron, E.C. (1977) Chromite in the central sector of the eastern Bushveld Complex, South Africa. Am. Mineral. 62:1082–1096

Cameron, E.C., Desborough, G.A. (1969) Occurrence and characteristics of chromite deposits – Eastern Bushveld Complex, South Africa, Econ. Geol. Monogr. 4:23–40

Cameron, E.C., Emerson, M.E. (1959) The origin of certain chromite deposits in the eastern part of the Bushveld Complex. Econ. Geol. 54:1151–1213

Campbell, I.H., Naldrett, A.J. (1979) The influence of silicate: sulfide ratios on the geochemistry of magmatic sulfides. Econ. Geol. 74:1503–1506

Campbell, I.H., Naldrett, A.J., Barnes, S.J. (1983) A model for the origin of the platinum-rich sulfide horizons in the Bushveld and Stillwater Complexes. J. Petrol. 24:133–165

Cousins, C.A., Feringa, G. (1964) The chromite deposits of the western Belt of the Bushveld Complex. In: Haughton, S.H. (ed.) The geology of some ore deposits in Southern Africa., vol. II. Geol. Soc. S. Afr. Johannesburg 183–202

Davies, G., Tredoux, M. (1985) Platinum-group element and gold contents of the marginal rocks and sills of the Bushveld Complex. Econ. Geol. 80:838–848

De Waal, S.A. (1975) The mineralogy, chemistry and certain aspects of reactivity of chromitite from the Bushveld Igneous Complex. S. Afr. Nat. Inst. Metallurgy Rep. 1709:80

Eales, H.V. (1987) Upper critical zone chromitite layers at R.P.M. Union Section Mine, western Bushveld Complex. In: Stowe, C.W. (ed.) Evolution of chromium ore fields. Van Nostrand Reinhold, Stroudsburg, Pennsylvania, pp. 144–168

Eales, H.V., De Klerk, W.J., Butcher, A.R., Kruger, F.J. (1990a) The cyclic unit beneath the UG1 chromitite (UG1FW unit) at RPM Union Section Platinum Mine – Rosetta Stone of the Bushveld Upper critical zone? Min. Mag. 54:23–43

Eales, H.V., De Klerk, Teigler, B. (1990b) Evidence for magma mixing processes within the critical and lower zones of the northwestern Bushveld Complex. Chem. Geol. 88:261–278

Eales, H.V., Field, M., De Klerk, W.J., Scoon, R.N. (1988) Regional trends of chemical variation and thermal erosion in the upper critical zone, western Bushveld complex. Min. Mag. 52:63–79

Eales, H.V., Maier, W.D., Teigler, B. (1991) Corroded plagioclase feldspar inclusions in orthopyroxenes and olivine of the lower and critical zones, western Bushveld Complex. Min. Mag. 55:479–486

Eales, H.V., Reynolds, I.M. (1986) Cryptic variations within chromitites of the upper critical zone, northwestern Bushveld Complex. Econ. Geol. 81:1056–1066

Eales, H.V., Reynolds, I.M., Gouws, D.A. (1980) The spinel-group minerals of the central Karoo tholeiitic province. Trans. Geol. Soc. S. Afr. 83:243–253

Griffith, J. (ed) (1989) South Africa's minerals – diversity in adversity. Industrial Minerals 263:18–53

Hatton, C.J., Von Gruenewaldt, G. (1987) The geological setting and petrogenesis of the Bushveld chromitite layers. In: Stowe, C.W. (ed) Evolution of chromium ore fields. Van Nostrand Reinhold, Stroudsburg, Pennsylvania, pp.: 109–143

Hiemstra, S.A. (1985) The distribution of some platinum-group elements in the UG-2 chromitite layer of the Bushveld Complex. Econ. Geol. 80:944–957

Hiemstra, S.A. (1986) The distribution of chalcophile and platinum-group elements in the UG-2 chromitite layer of the Bushveld Complex. Econ. Geol. 81:1080–1086

Hill, R., Roeder, P.L. (1974) The crystallization of spinel from basaltic liquid as a function of oxygen fugacity. J. Geol. 82:709–729

Irvine, T.N. (1965) Chromian spinel as a petrogenetic indicator. Can. J. Earth Sci. 2:648–672

Irvine, T.N. (1967) Chromian spinel as a petrogenetic indicator, Part 2. Petrologic applications. Can. J. Earth Sci. 4:71–103

Irvine, T.N. (1975) Crystallization sequences in the Muskox intrusion and other layered intrusions. II. Origin of chromitite layers and similar deposits of other magmatic ores. Geochim. Cosmochim. Acta 39:991–1020

Irvine, T.N. (1977) Origin of chromitite layers in the Muskox intrusion and other stratiform intrusions: a new interpretation. Geology 5:273–277

Irvine, T.N., Keith, D.W., Todd, S.G. (1983) The J-M Platinum – Palladium Reef of the Stillwater Complex, Montana. II. Origin by double-diffusive convective magma mixing and implications for the Bushveld Complex. Econ. Geol. 78:1287–1334

Lee, C.A., Parry, S.J. (1988) Platinum-group element geochemistry of the lower and middle group chromitites of the eastern Bushveld Complex. Econ. Geol. 83:1127–1139

Lee, C.A., Tredoux, M. (1986) Platinum-group element abundances in the lower and the lower critical zones of the eastern Bushveld Complex. Econ. Geol. 81:1087–1095

McDonald, J.A. (1967) Evolution of part of the lower critical zone, Farm Ruighoek, western Bushveld. J. Petrol. 8:165–209

Merkle, R.K.W. (1987) Platinum-group minerals in the middle group of chromitite layers at Marikana, western Bushveld Complex – Indications for collection mechanisms and postmagmatic modification. Inst. Geol. Res. Bushveld Complex, Research Report 66:32 pp.

Naldrett, A.J., Barnes, S.J. (1986) The behaviour of platinum group elements during fractional crystallization and partial melting with special reference to the composition of magmatic sulfide ores. Fortschr. Miner. 64:113–133

Naldrett, A.J., Cameron, G., Von Gruenewaldt, G., Sharpe, M.R. (1987) The formation of stratiform PGE deposits in layered intrusions. In Parsons, I. (ed.) Origins of igneous layering. Reichel, Dordrecht, pp. 313–397

Naldrett, A.J., Von Gruenewaldt, G. (1988) Association of platinum-group elements with chromitite in layered intrusions and ophiolite complexes. Econ. Geol. 84:180–187

Page, N.J. (1971) Comments on the role of oxygen fugacity in the formation of immiscible sulfide liquids in the H chromitite zone of the Stillwater Complex, Montana. Econ. Geol. 66:607–610

Roeder, P.L., Campbell, I.H. (1985) The effect of postcumulus reactions on composition of chome-spinels from the Jimberlana Intrusion. J. Petrol. 26:763–786

Scoates, R.F.J., Eckstrand, O.R., Cabri, L.J. (1988) Inter-element correlation, stratigraphic variation, and distribution of PGE in the ultramafic series of the Bird River sill, Canada. In: Prichard, H.M., Potts, P.J., Bowles, J.F.W., Cribb, S.J. (eds.) Geo-Platinum 87. Elsevier, Amsterdam New York Barking, pp. 239–249

Sharpe, M.R. (1982) Noble metals in the marginal rocks of the Bushveld Complex. Econ. Geol. 77:1286–1295

Silk, M.H. (1988) World chromite resources and ferrochromium production. Council for mineral technology. Spec. Publ. 11:149 pp.

Stockman, H.W., Hlava, P.F. (1984) Platinum-group minerals in alpine chromitites from southwestern Oregon. Econ. Geol. 79:491–508

South African Committee for Stratigraphy (SACS) (1980) Stratigraphy of South Africa, Part 1 (Comp.: L.E. Kent). Lithostratigraphy of the Republic of South Africa, South West Africa/Namibia, and the Republic of Bophuthatswana, Transkei and Venda. Geol. Survey of S. Afr. Handbook 8. (Pretoria):690 pp.

Talkington, W., Watkinson, D.H., Whittaker, P.J., Jones, P.C. (1983) Platinum-group-mineral inclusions in chromite from the Bird River Sill, Manitoba. Mineral. Deposita 18:245–255

Teigler, B. (1990a) Platinum group element distribution in the lower and middle group chromitites in the western Bushveld Complex. Mineralogy Petrology 42:165–179

Teigler, B. (1990b) Mineralogy, petrology and geochemistry of the Lower and lower Critical Zones, northwestern Bushveld Complex. Unpublished Ph.D. thesis, Rhodes University South Africa, 247 pp.

Ulmer, G.C. (1969) Experimental investigation of chromite spinels. Econ. Geol. Monogr. 4:114–131

Van Der Walt, C.F.J. (1941) Chrome ores of the western Bushveld Complex. Trans. Geol. Soc. Afr. 44:79–112

Van Zyl, J.P. (1970) The petrology of the Merensky Reef and the associated rocks on Swartklip 988, Rustenburg District. Geol. Soc. Afr. Spec. Publication 1:80–107

Vermaak, C.F. (1985) The UG2 layer – South Africa's slumbering chromitite giant. Chromium Review 5:9–22

Von Gruenewaldt, G., Hatton, C.J., Merkle, R.K.W., Gain, S.B. (1986) Platinum-Group Element – Chromitite associations in the Bushveld Complex. Econ. Geol. 81:1067–1079

Von Gruenewaldt, G., Worst, B.G. (1986) Chromite depostis at Zwartkop Chrome Mine, western Bushveld Complex. In: Anhaeusser, C.R., Maske, S. (eds.) Mineral deposits of Southern Africa, Vol. 2. Geol. Soc. S. Afr. 1217–1227

Wilson, A.H. (1982) The Geology of the Great Dyke, Zimbabwe: the ultramafic rocks. J. Petrol. 23:240–292

Editorial handling: DR